Poulos, T. L., Perez, M., & Wagner, G. C. (1982) *J. Biol. Chem. 257*, 10427–10429.
Poulos, T. L., Finzel, B. C., Gunsalus, I. C., Wagner, G. C., & Kraut, J. (1985) *J. Biol. Chem. 260*, 16122–16130.
Poulos, T. L., Finzel, B. C., & Howard, A. J. (1986) *Biochemistry 25*, 5314–5322.
Poulos, T. L., Finzel, B. C., & Howard, A. J. (1987) *J. Mol. Biol. 192*, 687–700.
Raag, R., & Poulos, T. L. (1989) *Biochemistry 28*, 917–922.
Shaanan, B. (1983) *J. Mol. Biol. 171*, 31–59.
Steigemann, W., & Weber, E. (1979) *J. Mol. Biol. 127*, 309–338.
Stern, J. O., & Peisach, J. (1974) *J. Biol. Chem. 249*, 7495–7498.
Uno, T., Nihsimura, Y., Makino, R., Iizuka, T., Ishimura, Y., & Tsuboi, M. (1985) *J. Biol. Chem. 260*, 2023–2026.
Wagner, G. C., & Gunsalus, I. C. (1982) in *The Biological Chemistry of Iron* (Dunford, H. B., Dolphin, D., Raymond, K., & Sieker, L., Eds.) pp 405–412, Riedel, Boston.
Wells, A. F. (1986) *Structural Inorganic Chemistry*, Oxford University Press, Oxford.
Yu, C. A., & Gunsalus, I. C. (1974) *J. Biol. Chem. 249*, 102–106.

Crystal Structure of Guanosine-Free Ribonuclease T_1, Complexed with Vanadate(V), Suggests Conformational Change upon Substrate Binding[†,‡]

Dirk Kostrewa, Hui-Woog Choe, Udo Heinemann, and Wolfram Saenger*
Institut für Kristallographie, Takustrasse 6, 1000 Berlin 33, FRG
Received January 25, 1989; Revised Manuscript Received May 1, 1989

ABSTRACT: Ribonuclease T_1 was crystallized in the presence of vanadate(V). The crystal structure was solved by molecular replacement and refined by least-squares methods using stereochemical restraints. The refinement was based on data between 10 and 1.8 Å and converged at a crystallographic R factor of 0.137. Except for the substrate-recognition site the three-dimensional structure of ribonuclease T_1 closely resembles the structure of the enzyme complexed with guanosine 2′-phosphate and its derivatives. A tetrahedral anion was found at the catalytic site and identified as $H_2VO_4^-$. This is the first crystal structure of ribonuclease T_1 determined in the absence of bound substrate analogue. Distinct structural differences between guanosine-free and complexed ribonuclease T_1 are observed at the base-recognition site: The side chains of Tyr45 and Glu46 and the region around Asn98 changed their conformations, and the peptide bond between Asn43 and Asn44 has turned around by 140°. We suggest that the structural differences seen in the crystal structures of free and complexed ribonuclease T_1 are related to conformational adjustments associated with the substrate binding process.

Ribonuclease T_1 (RNase T_1; EC 3.1.27.3) is an endoribonuclease secreted by the fungus *Aspergillus oryzae*. It cleaves RNA highly specifically at the 3′-phosphate group of guanylic acid. The enzyme occurs in two isoforms containing either Gln or Lys at position 25 (Gln25-RNase T_1 or Lys25-RNase T_1). Recently, several crystal structures of RNase T_1–substrate analogue complexes have been determined at high resolution: Gln25-RNase T_1*2′-GMP[1] (Sugio et al., 1985a, 1988), Lys25-RNase T_1*2′-GMP (Arni et al., 1987, 1988), Lys25-RNase T_1*G-(2′–5′)-pG (Koepke et al., 1989), and Gln25-RNase T_1*3′-GMP (Sugio et al., 1985b). However, the tertiary structure of substrate analogue free RNase T_1 was not known so far. Martin et al. (1980) described the crystallization of free RNase T_1, but a structure analysis was not reported. We had intended to cocrystallize RNase T_1 with guanosine–vanadate as a transition-state analogue but instead obtained the RNase T_1–vanadate complex, for reasons explained under Experimental Procedures. We report here the three-dimensional structure of guanosine-free Lys25-RNase T_1 and discuss the conformational differences between substrate analogue free Lys25-RNase T_1 and Lys25-RNase T_1 complexed with 2′-GMP, designated RNase T_1*2′-GMP.

Table I: X-ray Data

space group	$P2_12_12_1$ (No. 19)
lattice constants[a]	
a	48.82 (3) Å
b	46.53 (2) Å
c	41.20 (2) Å
total no. of measured reflections	11 536
$R_{sym} = \sum_h\sum_i\lvert\langle F_h\rangle - F_{h,i}\rvert/\sum_h\sum_i F_{h,i}$	0.029[b]
unique reflections	
$F_o \geq 1\sigma$	7134
$F_o \geq 3\sigma$	6503
completeness of data set at 1.8-Å resolution ($F_o \geq 1\sigma$)	
1.8-Å sphere	0.77
2.0–1.8-Å shell	0.59

[a] Numbers in parentheses are standard deviations and refer to the last digit. [b] Based on 1627 measurements in 804 unique reflections.

Experimental Procedures

Lys25-RNase T_1 was isolated by the method of Fülling and Rüterjans (1978). The guanosine–vanadate was prepared by

[†] This work was supported by the German Federal Minister for Research and Technology (BMFT) under Contract 05 313 IA B3, by the Deutsche Forschungsgemeinschaft through Sonderforschungsbereich 9 (Teilprojekt A7), and by the Fonds der Chemischen Industrie.
[‡] Crystal structure coordinates have been submitted to the Brookhaven Protein Data Bank.

[1] Abbreviations: 2′-GMP, guanosine 2′-phosphate; G-(2′–5′)-pG, guanylyl-(2′–5′)-guanosine; 3′-GMP, guanosine 3′-phosphate; rms, root mean square; Wat, water; MD, molecular dynamics.

0006-2960/89/0428-7592$01.50/0

heating the poorly soluble guanosine with NH_4VO_3 as described for the preparation of uridine–vanadate (Wlodawer et al., 1983). As determined later by IR spectroscopy (Zouni and Georgalis, personal communication), this treatment decomposes the guanosine to unknown fragments.

Single crystals were grown by microdialysis of 1–2% (w/v) RNase T_1 against a 10 mM sodium acetate buffer containing 2 mM $CaCl_2$, 1 mM NaN_3, the reaction product of the guanosine–vanadate synthesis, and 55% (v:v) 2-methyl-2,4-pentanediol as a precipitant, adjusted with acetic acid to a final pH $\approx$ 5. RNase T_1 crystallized as needle-shaped prisms in space group $P2_12_12_1$ with four molecules per unit cell. X-ray data were collected to 1.8-Å resolution on a diffractometer (details are given in Table I). The structure was solved with the molecular replacement method using the atomic coordinate set of RNase T_1 as present in the RNase T_1*2′-GMP complex (Arni et al., 1987, 1988) as a starting model. The cell constants of free RNase T_1 seemed sufficiently similar to those of RNase T_1*2′-GMP to directly proceed with refinement of the structure, when setting with $c < a < b$ was chosen. However, rigid body refinement against low-resolution data failed. Subsequent determination of the orientation of the model in the unit cell using the programs ALMN (Crowther, 1972) and SEARCH from the CCP4 program package (Machin et al., 1983) led to a 90° rotation around z of the model. For easy comparison with the 2′-GMP complex structure, the diffraction data were reindexed to yield the choice of axes given in Table I. The refinement of the structure was carried out with the fast Fourier transformation version PROFFT (Finzel, 1987; Sheriff, 1987) of the stereochemically restrained least-squares program PROLSQ (Hendrickson, 1985; Hendrickson & Konnert, 1980). Toward the end of refinement, the weights for the temperature factor restraints were decreased with respect to the originally proposed values (Hendrickson, 1985) according to an investigation of the role of temperature factor restraints in least-squares refinement by Yu et al. (1985). The refinement was guided by model building sessions with the computer graphics program FRODO (Jones, 1978, 1985) on the vector graphics system Evans & Sutherland PS 330. The mean error in atomic positions was estimated by the method of Luzzati (1952). A summary of refinement and weighting details is given in Table II.

Table II: Refinement

Starting Model	
atoms used	777 protein atoms from the RNase T_1*2′-GMP complex
orientation in unit cell found with programs	ALMN and SEARCH
initial R factor	0.42
Data Used in Refinement	
min resolution	10 Å
max resolution	1.8 Å
structure amplitudes	$F_o \geq 1\sigma$
no. of reflections used	7070
no. of refinement cycles	700
no. of model building sessions	29
final R factor	0.137
mean error in atomic positions	0.15 Å
rms electron density of F_o–F_c map	0.062 e^-/Å^3
final non-hydrogen atomic set	
RNase T_1	786 atoms
$H_2VO_4^-$	5 atoms
Ca^{2+}	1 atom
H_2O	162 atoms
Statistics of Final Structure[a]	
distance restraint information	
bond distance	0.025 (0.020) Å
angle distance	0.061 (0.050) Å
planar 1–4 distance	0.067 (0.050) Å
plane restraint information	
rms δ	0.012 (0.015) Å
chiral center restraints	
rms δ	0.249 (0.150) Å^3
nonbonded contact restraints	
single-torsion contact	0.131 (0.150) Å
multiple-torsion contact	0.138 (0.150) Å
possible (X–Y) hydrogen bond	0.158 (0.150) Å
conformational torsion angles	
planar	1.9 (3.0)°
staggered	20.0 (15.0)°
orthonormal	22.8 (20.0)°
isotropic thermal factor restraints	
main-chain bond	2.123 (2.000) Å^2
main-chain angle	2.698 (3.000) Å^2
side-chain bond	4.706 (4.500) Å^2
side-chain angle	6.034 (6.000) Å^2
hydrogen bond	15.136 (15.000) Å^2
diffraction data	
structure factor modulus	$\sigma_F \simeq 0.5 \langle \|\|F_{obs}\| - \|F_{calc}\|\| \rangle$

[a] Target restraints in parentheses.

Results

Refinement Results. The final atomic coordinate set contains 776 protein atoms in fully occupied positions, 5 protein atoms in the side chains of Val78 ($C\gamma_1$, $C\gamma_2$) and Asn 98 ($C\gamma$, $C\delta_1$, $N\delta_2$) in two alternate positions, 160 water molecules, 2 of which are disordered, 1 calcium ion, and 5 vanadate(V) atoms. The electron density for all amino acids was clearly defined with the exception of the side chain of Asn98, where in two disordered conformations only one δ atom could be detected. A problem arose with a bulky electron density with a vague tetrahedral shape positioned in the catalytic site. Trials to fit NH_4^+ or acetic acid into the electron density failed, because of residual electron density difference occurring above and below the acetic acid plane or spherically around the NH_4^+, even at artificial temperature factors close to zero. Only calcium or chloride ion could fit the observed electron density with a reasonable temperature factor, but they "hovered" in the structure without any coordination contact to other atoms. Considering the vanadium chemistry, we found that the most abundant monomeric species of vanadium(V) ion in water at the pH of crystallization is $H_2VO_4^-$, with probable tetrahedral structure (Pope & Dale, 1968). An ideal group of $H_2VO_4^-$ was taken from the crystal structure of NH_4VO_3, where the vanadate crystallized in the form of a polymeric tetrahedral chain (Evans, 1960) with each vanadium atom surrounded by four oxygen atoms to build a distorted tetrahedron. The ideal $H_2VO_4^-$ group without hydrogen atoms was defined as an ideal tetrahedron with an average V–O bond length of 1.73 Å, since it was impossible to distinguish in the electron density map between the slightly varying V–O distances expected from the NH_4VO_3 study. In subsequent cycles of refinement no restraints were put on the bond angles and the vanadate group maintained its tetrahedral stereochemistry. The final vanadate group shows a distorted tetrahedral structure and two V–O bonds slightly shorter than the other two. The four oxygen atoms are involved in eleven hydrogen bonds with good stereochemistry to all amino acids of the catalytic site. The temperature factors of the vanadate group are higher than the mean temperature factor of B = 20 Å^2,

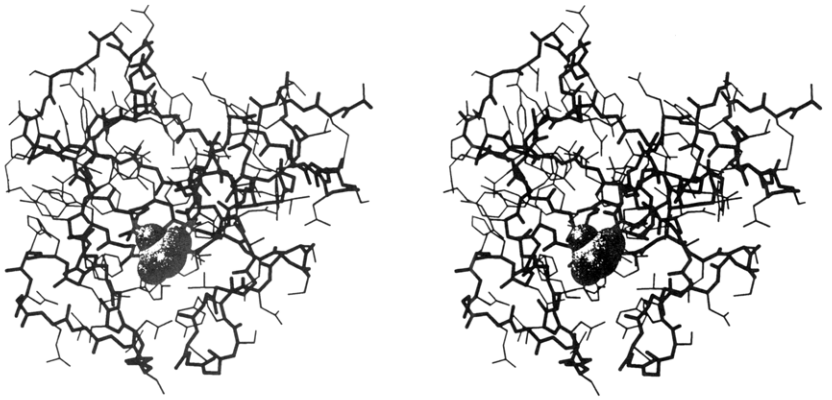

FIGURE 1: Stereoview of RNase T_1*$H_2VO_4^-$, with main chain in thick lines, side chains (main conformation) in thin lines, and vanadate as space-filling group. Stereographic drawings were performed with SCHAKAL 88 (Keller, 1988).

Table III: Crystal Contacts

possible hydrogen bond	distance (Å)	D–Ĥ···A (deg)	symmetry operation[a]
Ala1 N ↔ O His92	3.1		$-x + {}^1/_2, -y, z + {}^1/_2$
Ala1 N ↔ O Ala95	2.8		$-x + {}^1/_2, -y, z + {}^1/_2$
Ala1 O ↔ N Gly94	3.3	137	$-x + {}^1/_2, -y, z + {}^1/_2$
Asn9 $O\delta_1$ ↔ $O\epsilon_1$ Glu31	2.5		$-x + 1, y - {}^1/_2, -z + {}^1/_2$
Asn9 $O\delta_1$ ↔ $O\epsilon_2$ Glu31	3.2		$-x + 1, y - {}^1/_2, -z + {}^1/_2$
Asn9 $N\delta_2$ ↔ $O\epsilon_2$ Glu31	2.7	144	$-x + 1, y - {}^1/_2, -z + {}^1/_2$
Glu28 $O\epsilon_1$ ↔ N Asn44	3.3	136	$-x + {}^1/_2, -y + 1, z + {}^1/_2$
Glu28 O ↔ Oγ Ser72	2.7		$-x + 1, y + {}^1/_2, -z + {}^1/_2$
Thr32 N ↔ Oγ Ser63	3.1	123	$-x + 1, y + {}^1/_2, -z + {}^1/_2$
Thr32 $O\gamma_1$ ↔ Oγ Ser63	2.9		$-x + u, y + {}^1/_2, -z + {}^1/_2$
Ser35 Oγ ↔ $O\epsilon_2$ Glu46	3.2		$x + {}^1/_2, -y + {}^1/_2 - z$
Ser35 Oγ ↔ O Phe100	2.8		$x + {}^1/_2, -y + {}^1/_2, -z$
Asp49 $O\delta_1$ ↔ $N\delta_2$ Asn98	2.6	126	$x - {}^1/_2, -y + {}^1/_2, -z$

[a] Symmetry-equivalent atoms are on the right side of each possible hydrogen bond.

with the *B* value of vanadium being ≈40 Å^2 and that of the oxygens ≈45 Å^2. The difference between the temperature factors of vanadium and the bound oxygens is probably due to the decreased temperature factor restraints and more so to an oscillation of the oxygen positions with vanadium as a center of mass. Lower temperature factors could have been forced by decreasing the occupancy below 1.0.

A secondary structure analysis of the guanosine-free RNase T_1 was carried out with the program DSSP (Kabsch & Sander, 1983). The complete tertiary structure of the enzyme with all side chains in their main conformation is presented in Figure 1 (without bound calcium cation and water molecules). For analysis of hydrogen-bonding interactions, hydrogen atoms covalently bonded to sp^2-hybridized nitrogen atoms were added in both structures with programs MOLEDT for amino acids and INSIGHT for guanine from the Molecular Modelling System (1987) of BIOSYM. These hydrogen atoms were included in the calculation of hydrogen bonds. Possible hydrogen bonds have donor–acceptor (D–A) distances ≤3.5 Å, hydrogen–acceptor distances ≤2.5 Å, and angles D–Ĥ···A ≥90°.

Table III gives possible hydrogen bonds between protein molecules in the crystal lattice. A similar compilation of lattice contacts in crystals of the RNase T_1*2′-GMP may be found in Arni et al. (1987). Intermolecular contacts in both crystal forms are similar, bringing in close contact equivalent surface regions of RNase T_1 molecules. Three intermolecular hydrogen bonds are identical in the two crystals, while in several cases surface residues engage in hydrogen bonds to side chains in the vicinity of their partners in the other crystal form. Interestingly, the intermolecular hydrogen bonds Ala1 O–Gly94 N and Asp49 $O\delta_1$–Asn98 $N\delta_2$ of free RNase T_1 are mediated by a bridging water molecule in the inhibitor complex. Although a few lattice contacts are unique in free RNase T_1, it is unlikely that the conformation of the protein is significantly altered by the slightly different crystal packing.

*Comparison of Guanosine-Free RNase T_1 with RNase T_1*2′-GMP Complex.* To facilitate the comparison between guanosine-free RNase T_1 and the structure of RNase T_1 complexed with 2′-GMP, a two-step least-squares fit of the latter coordinates on the former was performed. In the first step, the transformation for all main-chain atoms was calculated. In the second step, only those main-chain atoms were considered in the calculation which deviated not more than one rms deviation in the structure comparison of the first step. This final transformation was applied to the whole atomic coordinate set of the RNase T_1*2′-GMP complex. This selected least-squares fit procedure was choosen to avoid weighting on the largest differences in both structures which would have obscured the structural differences and to achieve a maximum overlay of the structurally conserved parts. After the coordinate transformation, the rms difference for the main-chain atoms was 0.47 Å, for side-chain atoms 1.07 Å, and for all protein atoms 0.80 Å. The differences are statistically significant compared to the mean error in atomic positions (see Table II).

The rms deviations between both structures of main-chain and side-chain atoms are shown in Figure 2 for each amino acid. We would like to focus first on the deviations of the main-chain atoms. It is striking that the largest deviations occur in the two base-recognition loops from amino acid 43 to 55 and from 92 to 100. Although amino acids 47–50 are not directly involved in base recognition, the main-chain atoms of Phe48 are hydrogen bonded to the side chain of Asn44 and therefore also shifted in their positions. The amino acids adjacent to Asn98 are part of the second base-recognition loop which has also altered its conformation.

An analysis of the Φ and Ψ backbone torsion angles shows that one peptide group has turned around by 140°, namely,

Table IV: Comparison of Hydrogen-Bonding Interactions in Catalytic Sites

group	RNase T_1*$H_2VO_4^-$	distance (Å)	D–Ĥ···A (deg)	RNase T_1*2′-GMP	distance	D–Ĥ···A (deg)
His40	$N\epsilon_2 \leftrightarrow O_3$–V	3.0	137	$N\epsilon_2 \leftrightarrow O_1$–P	2.8	169
	$N\epsilon_2 \leftrightarrow$ Wat176	3.0	125			
Glu58	$O\epsilon_1 \leftrightarrow O_4$–V	2.7		$O\epsilon_1 \leftrightarrow O_3$–P	2.7	
	$O\epsilon_1 \leftrightarrow$ Wat175	2.7		$O\epsilon_2 \leftrightarrow O_1$–P	3.4	
	$O\epsilon_2 \leftrightarrow O_2$–V	2.9		$O\epsilon_2 \leftrightarrow O_3$–P	2.4	
	$O\epsilon_2 \leftrightarrow O_4$–V	3.1		$O\epsilon_2 \leftrightarrow N\epsilon$ 77	3.2	129
Arg77	$N\epsilon \leftrightarrow O_2$–V	2.6	143	$N\epsilon \leftrightarrow O\epsilon_2$ 58	3.2	129
	$N\eta_2 \leftrightarrow$ Wat199	2.8	116	$N\eta_2 \leftrightarrow$ Wat130	2.8	134
	$N\eta_2 \leftrightarrow O_2$–V	3.2	133			
His92	$N\epsilon_2 \leftrightarrow O_2$–V	2.8	135	$N\epsilon_2 \leftrightarrow$ O 98	3.0	121
Asn98	$O\delta_1 \leftrightarrow O_1$–V	3.1		$N\delta_2 \leftrightarrow$ Wat186	3.0	140
	$O\delta_1 \leftrightarrow$ Wat183	2.8		$N\delta_2 \leftrightarrow$ Wat158	2.3	108
				O $\leftrightarrow N\epsilon_2$ 92	3.0	121
				O $\leftrightarrow N_2$ 2′-GMP	2.9	145
				O $\leftrightarrow$ Wat158	3.2	
$H_2VO_4^-$	V–$O_1 \leftrightarrow O\delta_1$ 98	3.1				
	V–$O_1 \leftrightarrow$ Wat183	2.8				
	V–$O_2 \leftrightarrow O\epsilon_2$ 58	2.9				
	V–$O_2 \leftrightarrow N\epsilon$ 77	2.6	143			
	V–$O_2 \leftrightarrow N\eta_2$ 77	3.2	133			
	V–$O_2 \leftrightarrow N\epsilon_2$ 92	2.8	135			
	V–$O_3 \leftrightarrow N\epsilon_2$ 40	3.0	137			
	V–$O_3 \leftrightarrow$ Wat176	2.6				
	V–$O_4 \leftrightarrow O\epsilon_1$ 58	2.7				
	V–$O_4 \leftrightarrow O\epsilon_2$ 58	3.1				
	V–$O_4 \leftrightarrow$ Wat175	2.8				
2′-GMP				$N_2 \leftrightarrow$ O 98	2.9	145
				$N_3 \leftrightarrow O_{5'}$	2.7	
				$O_{2'} \leftrightarrow$ Wat148	3.5	
				$O_{3'} \leftrightarrow$ Wat148	3.5	
				$O_{5'} \leftrightarrow$ Wat158	2.8	
				P–$O_1 \leftrightarrow N\epsilon_2$ 40	2.8	169
				P–$O_1 \leftrightarrow O\epsilon_2$ 58	3.4	
				P–$O_2 \leftrightarrow$ Wat158	2.6	
				P–$O_2 \leftrightarrow$ Wat179	3.0	
				P–$O_2 \leftrightarrow$ Wat186	2.7	
				P–$O_3 \leftrightarrow O\epsilon_1$ 58	2.7	
				P–$O_3 \leftrightarrow O\epsilon_2$ 58	2.4	
water	Wat183 $\leftrightarrow$ Wat199	3.0		Wat130 $\leftrightarrow$ Wat186	3.2	
				Wat179 $\leftrightarrow$ Wat186	2.7	

the peptide bond between Asn43 and Asn44, which also is directly involved in base recognition (Asn43 Ψ/Asn44 Φ: −14°/61° in RNase T_1*2′-GMP and 126°/−81° in free RNase T_1).

Nearly all changes in side-chain conformation occur in loop regions and are associated either with side chains at the periphery of RNase T_1 or with altered conformations at the base-recognition site.

The temperature factors of RNase T_1*$H_2VO_4^-$ and of RNase T_1*2′-GMP are compared in Figure 3. The largest values for main-chain atoms and even more so for side-chain atoms occur in the loop regions. This is especially obvious in the guanosine-free enzyme where the largest temperature factors for main- and side-chain atoms occur in both base-recognition loops. These effects cannot be explained with the reduced temperature factor restraints of the free enzyme, since this would have affected all temperature factors equally.

Structural Differences at the Catalytic Site. The structural details of the catalytic sites are shown in Figure 4: The side chains of His40, Glu58, and Arg77 nearly adopt the same conformations in both structures. The His92 ring is turned around in the vanadate complex to facilitate better hydrogen-bonding interaction. The side chain of Asn98 is also turned around to achieve a maximum number of hydrogen-bonding interactions. The vanadium and phosphorus positions are nearly identical, but the oxygens are in different positions. The vanadate group replaces every hydrogen bond of the phosphate group and exhibits six additional hydrogen bonds. Three water molecules are in equivalent positions: Wat176, Wat183, and Wat199 of the vanadate complex and Wat148, Wat186, and Wat130 of the 2′-GMP complex, respectively. A detailed analysis of hydrogen-bonding interactions in the

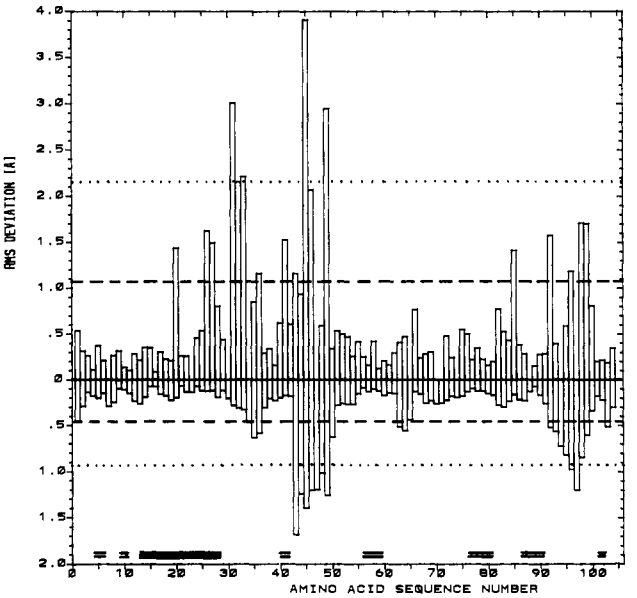

FIGURE 2: rms deviation between RNase T_1*$H_2VO_4^-$ and RNase T_1*2′-GMP for side-chain atoms (above) and main-chain atoms (below). 1 × rms deviations are marked (---), 2 × rms deviations are marked (···), α-helix is underscored (■), and β-sheets are underscored (═).

Table V: Comparison of Hydrogen-Bonding Interactions in Base-Recognition Sites

group	RNase T_1*$H_2VO_4^-$	distance (Å)	D–Ĥ···A (deg)	RNase T_1*2′-GMP	distance (Å)	D–Ĥ···A (deg)
Tyr42	Oη ↔ Wat179	2.7		Oη ↔ Oε$_1$ 46	3.1	
	Oη ↔ Oδ$_1$ 44	3.0				
Asn43	N ↔ Wat139	2.9	171	N ↔ N$_7$ 2′-GMP	3.3	169
	O ↔ N 45	2.8	137			
	O ↔ Wat139	3.4				
	O ↔ Wat179	2.9				
Asn44	Oδ$_1$ ↔ Oη 42	3.0		N ↔ O$_6$ 2′-GMP	2.8	106
Tyr45	N ↔ O 43	2.8	137	N ↔ O$_6$ 2′-GMP	2.8	155
	Oη ↔ O 98	3.4				
	Oη ↔ Wat177	2.8				
Glu46	N ↔ Wat179	3.2	158	N ↔ Oε$_1$	2.8	142
				Oε$_1$ ↔ Oη 42	3.1	
				Oε$_1$ ↔ N$_1$ 2′-GMP	2.7	161
				Oε$_2$ ↔ N$_2$ 2′-GMP	3.0	168
Asn98	O ↔ Oη 45	3.4		O ↔ N$_2$ 2′-GMP	2.9	145
	O ↔ Wat177	3.3		O ↔ Wat158	3.3	
				Nδ$_2$ ↔ Wat158	2.3	108
2′-GMP				N$_1$ ↔ Oε$_1$ 46	2.7	161
				N$_2$ ↔ Oε$_2$ 46	3.0	168
				N$_2$ ↔ O 98	2.9	145
				N$_7$ ↔ N 43	3.3	169
				O$_6$ ↔ N 44	2.8	106
				O$_6$ ↔ N 45	2.8	155
				O$_{5'}$ ↔ Wat 158	2.8	
water	Wat139 ↔ Wat175	2.6				
	Wat139 ↔ Wat177	3.3				
	Wat175 ↔ Wat177	2.9				

Table VI: Additional Hydrogen-Bonding Interactions in Catalytic and Base-Recognition Sites

group	RNase T_1*$H_2VO_4^-$	distance (Å)	D–Ĥ···A (deg)	RNase T_1*2′-GMP	distance (Å)	D–Ĥ···A (deg)
His40	Nδ$_1$ ↔ O 41	3.2	170	Nδ$_1$ ↔ O 41	2.8	149
Arg77	Nη$_1$ ↔ O 76	2.9	154	Nη$_1$ ↔ O 76	3.0	155
	Nη$_1$ ↔ O 74	3.0	141	Nη$_1$ ↔ O 74	3.0	159
	Nη$_2$ ↔ O 74	3.1	155			
His92	Nδ$_1$ ↔ O 99	2.8	158			
Tyr42	O ↔ Wat110	2.6		O ↔ Wat122	2.7	
	N ↔ O 56	2.9	161	N ↔ O 56	2.8	169
Asn43	Oδ$_1$ ↔ Wat186	2.7		Oδ$_1$ ↔ Wat 187	3.1	
	Nδ$_2$ ↔ Wat230	2.7	108	Nδ$_2$ ↔ Wat187	3.1	147
	Nδ$_2$ ↔ Wat250	3.4	150	O ↔ Wat183[b]	3.4	
Asn44	O ↔ N 47	3.1	157	O ↔ N 47	3.1	143
	N ↔ Wat137	2.9	155	O ↔ Wat183[b]	2.5	
	Oδ$_1$ ↔ N 48	3.3	156	Oδ$_1$ ↔ N 48	3.2	149
	Nδ$_2$ ↔ O 48	2.9	165	Nδ$_2$ ↔ O 48	2.9	164
Tyr45	O ↔ Wat151	2.6		O ↔ Wat137	2.7	
	Oη ↔ Wat246	3.4		Oη ↔ Nδ$_2$ 83[b]	2.7	141
Glu46	O ↔ Wat135	2.7		O ↔ Wat120[c]	2.8	
	Oε$_2$ ↔ Nδ$_2$ 99	3.0	148	O ↔ Wat129[c]	3.0	
	Oε$_1$ ↔ N 100	2.8	147	Oε$_2$ ↔ N 100	3.1	138
Asn98	Nδ$_2$ ↔ Oδ$_1$ 49[a]	2.6	126	Oδ$_1$ ↔ Wat124[d]	2.5	
$H_2VO_4^-$	V–O$_1$ ↔ Wat266	3.3				
	V–O$_3$ ↔ Oη 38	2.6				
2′-GMP				P–O$_1$ ↔ Oη 38	2.7	

[a] $x + 1/2, -y, +1/2, -z$. [b] $-x + 1/2, -y + 1, z + 1/2$. [c] $x - 1/2, -y + 1 1/2, -z + 1$. [d] $x + 1/2, -y + 1 1/2, -z + 1$.

catalytic sites is given in Table IV. The side-chain positions of His40, His92 (only in the vanadate complex), and especially Arg77 are stabilized by hydrogen bonding to main-chain oxygens of Lys41, Gly74, and Asp76.

Structural Differences at the Base-Recognition Site. The structural details of the base-recognition sites are shown in Figure 5. A detailed analysis of hydrogen-bonding interactions in base-recognition sites of RNase T_1*$H_2VO_4^-$ and RNase T_1*2′-GMP is given in Table V. Hydrogen-bonding interactions to neighboring amino acids and water for catalytic and base-recognition sites may be taken from Table VI.

In the vanadate complex, a few water molecules occupy the guanosine binding site. Residue Tyr42 is in the same position in both structures; its phenolic hydroxyl group forms two hydrogen bonds to Wat179 and to Oδ$_1$ of Asn44 in the vanadate complex and one hydrogen bond to Oε$_1$ of Glu46 in the 2′-GMP complex, which is in an equivalent position to Wat179 in the vanadate complex. The peptide bond between Asn43 and Asn44 has turned around by 140° in the vanadate complex with respect to the 2′-GMP complex. In the vanadate complex, the main-chain nitrogen of Asn43 takes part in one hydrogen bond to Wat137 and in one hydrogen bond to O$_6$ of guanine in the 2′-GMP complex. The main-chain oxygen of Asn43 in the vanadate complex is stabilized by three hydrogen bonds to Tyr45 N, Wat139, and Wat179, whereas in the 2′-GMP complex the main-chain oxygen of Asn43 takes part in only one hydrogen bond to Wat183. The side chain shows only hydrogen bonding to water molecules, i.e., one hydrogen bond between Asn43 Oδ$_1$ and Wat186 and one between Asn43 Nδ$_2$ and Wat230 in the vanadate complex, which replace two hydrogen bonds between Asn43 Oδ$_1$ and Wat187 and Asn43 Nδ$_2$ and Wat187 in the 2′-GMP complex.

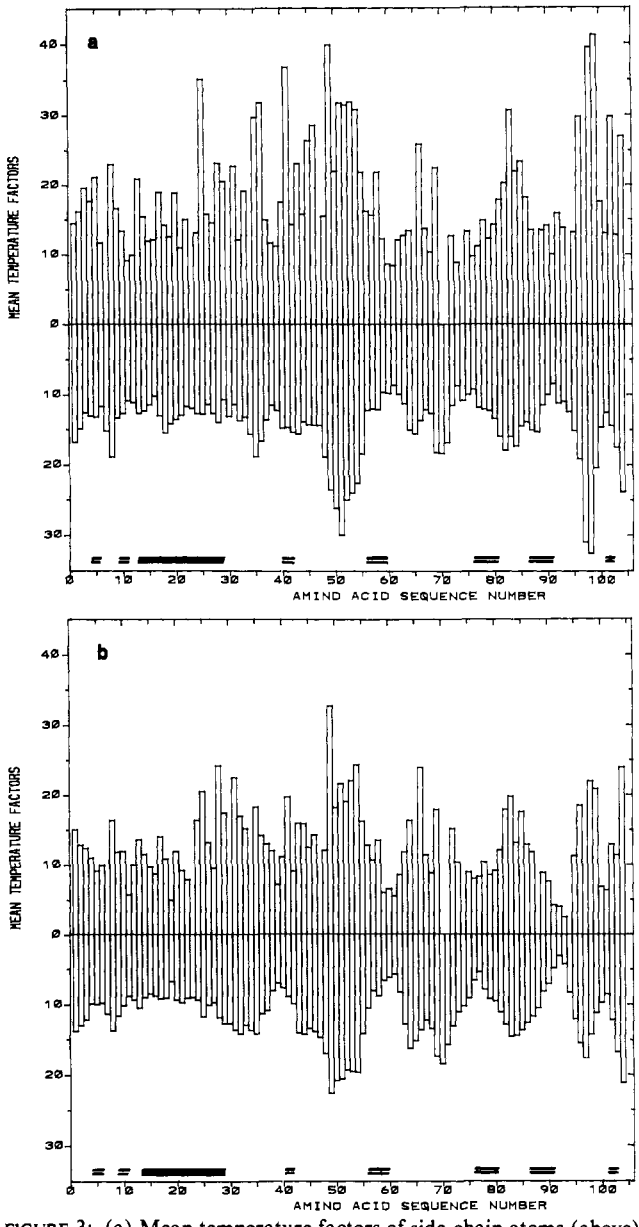

FIGURE 3: (a) Mean temperature factors of side-chain atoms (above) and main-chain atoms (below) of RNase T_1*$H_2VO_4^-$. α-Helix is underscored (■), and β-sheets are underscored (=). (b) Mean temperature factors of side-chain atoms (above) and main-chain atoms (below) of RNase T_1*2′-GMP. α-Helix is underscored (■), and β-sheets are underscored (=).

One additional hydrogen bond from Asn43 $N\delta_2$ to Wat250 is observed in the vanadate complex.

The main-chain nitrogen of Asn44 engages in one hydrogen bond to Wat137 in the vanadate complex and one hydrogen bond to O_6 of guanine in the 2′-GMP complex, respectively. The side chain of Asn44 shows a similar hydrogen-bonding pattern in both structures: There is one hydrogen bond between $O\delta_1$ and the main-chain nitrogen of Phe48 and one hydrogen bond between $N\delta_2$ and the main-chain oxygen of Phe48 in each structure. One additional hydrogen bond from Asn44 $O\delta_1$ to the phenolic hydroxyl group of Tyr42 is found in the vanadate complex. Thus, the stabilization of loop conformation by the Asn44 amide group remains much the same in both structures.

While the main chain of Tyr45 adopts the same conformation in both structures, its side chain has altered its conformation and takes part in completely different interactions. In the 2′-GMP complex, the phenolic ring of Tyr45 is the lid of a sandwich-like complex with O_6 of guanine in the middle and the phenolic ring of Tyr42 at the bottom. The phenolic hydroxyl group of Tyr45 takes part in only one hydrogen bond to a symmetry-equivalent Asn83 $N\delta_2$. In the vanadate complex, the phenolic ring of Tyr45 is turned away and stabilized by three hydrogen bonds to Wat177, Wat246, and the main-chain oxygen of Asn98, which replaces the amino group of guanine of the 2′-GMP complex.

The main-chain nitrogen of Glu46 shows one hydrogen bond to Wat179 in the vanadate complex and one hydrogen bond to $O\epsilon_1$ of Glu46 in the 2′-GMP complex. The side chain of Glu46 is also turned away in the vanadate complex with respect to the 2′-GMP complex. Both carboxylate oxygens exhibit five hydrogen bonds in the 2′-GMP complex, two of them to N_1 and N_2 of guanine and three to Glu46 N, Tyr42 $O\eta$, and Phe100 N. In the vanadate complex, both carboxylate oxygens are fixed by hydrogen bonding from $O\epsilon_2$ to Asn99 $N\delta_2$ and from $O\epsilon_1$ to Phe100 N, where the $O\epsilon_1$ replaces the $O\epsilon_2$ of the 2′-GMP complex in its interaction to Phe100 N, yielding a more stable hydrogen bond.

In the vanadate complex, the main-chain oxygen of Asn98 is hydrogen bonded to two donor groups, i.e., Tyr45 $O\eta$ and Wat177, where Tyr45 $O\eta$ replaces N_2 of guanine in the 2′-GMP complex. In the 2′-GMP complex, the main-chain oxygen is hydrogen bonded to guanine N_2, Wat158, and His92 $N\epsilon_2$. The side-chain $O\delta_1$ shows two hydrogen bonds to the vanadate V–O_1 and to Wat183 in the vanadate complex and one hydrogen bond to Wat124 in the 2′-GMP complex. The side-chain amide nitrogen forms one hydrogen bond from $N\delta_2$ to a symmetry-equivalent position of Asp49 $O\delta_1$ in the vanadate complex and two hydrogen bonds from $N\delta_2$ to Wat186 and from $N\delta_2$ to Wat158 in the 2′-GMP complex.

Cation Binding Site. Interestingly, the same calcium binding site was found as in the RNase T_1*G-(2′–5′)-pG complex (Koepke et al., 1989). The calcium ion is coordinated to two carboxylate oxygens of Asp15 and six water molecules. Oxygens of the coordination sphere engage in intensive hydrogen bonding to Ser12 $O\gamma$, Ser12 N, three main-chain oxygens of Cys10, Ser63, and a symmetry-equivalent Gly94 as well as two water molecules (Figure 6). These interactions could explain why Asp15 is a preferred and unique Ca^{2+} binding site in the crystal. Since only one hydrogen bond is promoted by crystal packing, we believe that Asp15 is a Ca^{2+} binding site in solution as well. The existence of specific ion binding sites in RNase T_1 has been demonstrated (Pace & Grimsley, 1988).

Discussion

Are the conformational differences between guanosine-free RNase T_1 and RNase T_1 complexed with 2′-GMP related to structural rearrangements during inhibitor binding? In principle, structural differences could also arise from the slightly different crystal packing. At the base-recognition site, a number of distinct changes are observed: (1) At least four water molecules found in the vanadate complex are replaced by the substrate. (2) The peptide bond between Asn43 and Asn44 has turned around to facilitate hydrogen bonding to the guanine O_6. (3) The Tyr45 ring has swung over to build a sandwich-like complex with guanine O_6 in the middle and Tyr42 on opposite site. (4) The Glu46 side chain has flipped around to lock the base in its position by two strong hydrogen bonds to N_1 and N_2. (5) The position of Asn98 has shifted toward the amino group of guanine.

Of these, the change in position and mobility (see below) of the Tyr45 side chain may be related to the crystalline environment since, in both RNase T_1*2′-GMP and RNase

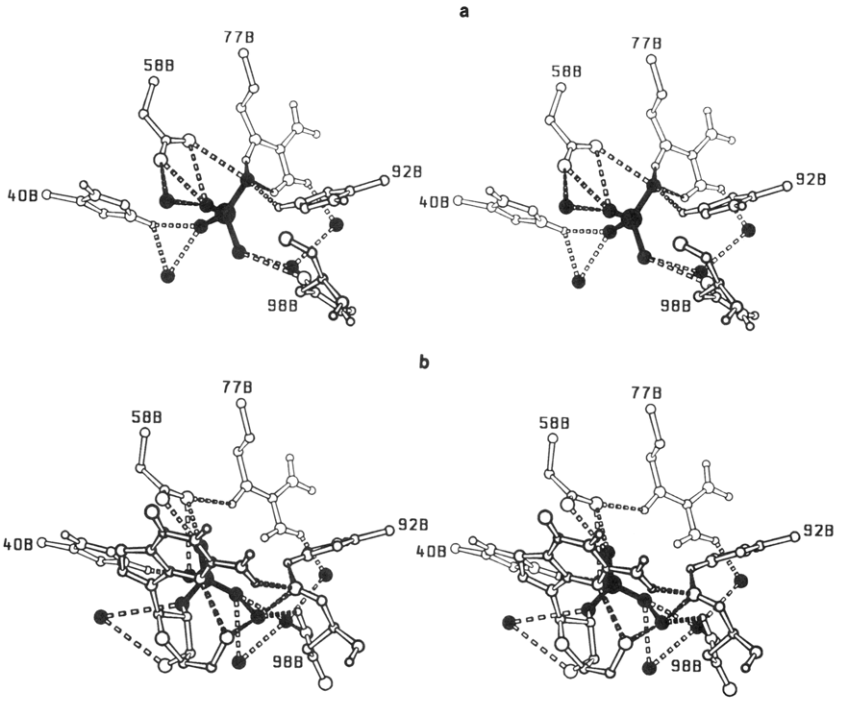

FIGURE 4: (a) Catalytic site of RNase T_1*$H_2VO_4^-$. Cβ atoms are labeled, and vanadate group and water molecules are filled. (b) Catalytic site of RNase T_1*2′-GMP. Cβ atoms are labeled, and phosphate group and water molecules are filled.

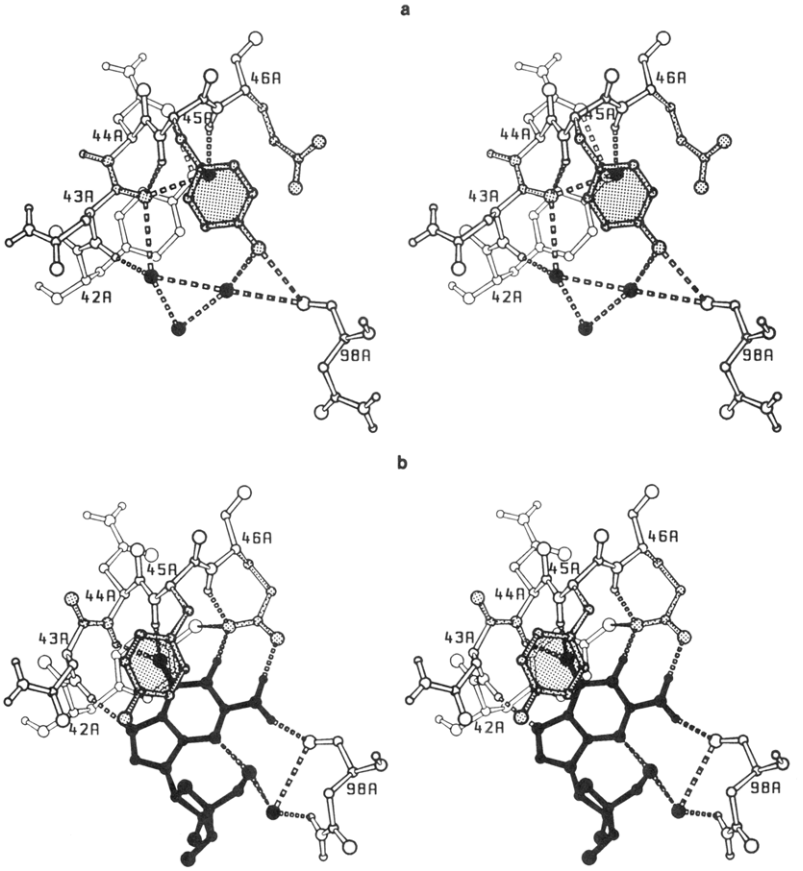

FIGURE 5: (a) Base-recognition site of RNase T_1*$H_2VO_4^-$. Cα atoms are labeled, water molecules are filled, and main structural changes to RNase T_1*2′-GMP are stippled. (b) Base-recognition site of RNase T_1*2′-GMP. Cα atoms are labeled, 2′-GMP and water molecules are filled, and main structural changes to RNase T_1*$H_2VO_4^-$ are stippled.

T_1*G-(2′–5′)-pG, intermolecular hydrogen bonding of the phenolic hydroxyl group is observed (Arni et al., 1987; Koepke et al., 1989) which is absent in the present structure. The Tyr45 phenolic ring shows a restricted flexibility in the free RNase T_1 compared to the 2′-GMP complex in ^{1}H NMR measurements (Rüterjans, personal communication). On one hand, this is consistent with the increased number of three hydrogen bonds to the Tyr45 Oη in the guanosine-free RNase T_1 compared to one intermolecular hydrogen bond to this atom and one stacking interaction with a negatively polarized O_6

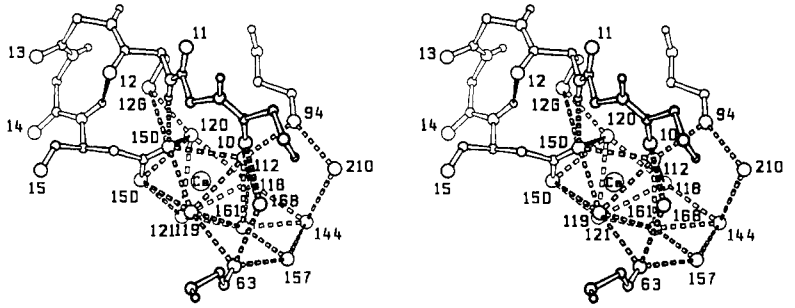

FIGURE 6: Calcium binding site of RNase T_1*$H_2VO_4^-$. Only those side-chain atoms are shown which are involved in calcium binding. Gly94 is symmetry-related with $(-x + {}^1/_2, -y + 2, z - {}^1/_2)$. The calcium ion and all oxygen atoms are labeled.

of guanine and Tyr42 in the 2′-GMP complex. On the other hand, the temperature factor of the Tyr45 side chain is twice as high in the guanosine-free RNase T_1 as in the 2′-GMP complex, which may indicate an increased mobility in the free enzyme.

Contradictory to the X-ray results, the Tyr45 side chain in the molecular dynamics calculations is not turned away in the free enzyme but is shifted along the Cβ-Cγ axis to lead to a more open base binding site. Thus, regarding the possible conformational change of the Tyr45 side chain, the agreement of the X-ray work with NMR and theoretical results is incomplete. In contrast, the remaining differences in recognition site geometry between free and complexed RNase T_1 are generally consistent with recent NMR and MD work. Therefore, we believe that the structural differences seen in the crystal structures are relevant to RNase T_1 in aqueous solution and to conformational rearrangements during substrate binding.

The rotation of the peptide bond between Asn43 and Asn44 has to be facilitated by elevated local flexibility. This is supported by ^{1}H NMR measurements, where the peptide hydrogen of Asn44 could not be detected in the spectra of free RNase T_1 and RNase T_1 complexed with 2′-GMP, probably due to fast motion of that peptide bond (Rüterjans, personal communication). Molecular dynamics calculations have been performed on RNase T_1 complexed with 2′-GMP and free RNase T_1 both starting from the structure of the RNase T_1*2′-GMP complex (Arni et al., 1988). There is a fair correlation of the rms fluctuation of free RNase T_1 in the MD calculation (MacKerell et al., 1988) and the observed temperature factors of guanosine-free RNase T_1 in the crystal structure. The rms difference of free RNase T_1 and RNase T_1 complexed with 2′-GMP in the MD calculations (MacKerell, personal communication) shows good correlation to the rms difference between the crystal structures as shown in Figure 2. The calculations predict the turnaround of the peptide bond between Asn43 and Asn44 in the free enzyme, a shift of Asn98 toward the base in the 2′-GMP complex, and a flip of the Glu46 side chain away from the base position in the free enzyme, although its magnitude is higher in the crystal structures. Overall, the MD calculations predict a more open active site in free RNase T_1 compared with the enzyme containing bound 2′-GMP.

Looking at all the structural adjustments in the base-recognition site during substrate binding which are apparent from the crystal structures of guanosine-free RNase T_1 and RNase T_1 complexed with 2′-GMP, we would like to propose a "snap-in" mechanism rather than an "open–close" mechanism for the substrate binding process of RNase T_1. A snap-in mechanism would involve distinct conformational adjustments of the enzyme, leading to altered hydrogen bonding of active site residues within the protein. These changes can be clearly seen for the Asn43–Asn44 peptide group and the side chain of Glu46. They are not accompanied by a contraction/expansion motion of the active site crevice.

Acknowledgments

We are grateful to H. Rüterjans and A. MacKerell for the communication of results prior to publication. Technical assistance of M. Steifa and help with refinement programs by J. Koepke and Molecular Modelling programs by U. Egner are gratefully acknowledged.

References

Arni, R., Heinemann, U., Maslowska, M., Tokuoka, R., & Saenger, W. (1987) *Acta Crystallogr. B43*, 548–554.

Arni, R., Heinemann, U., Tokuoka, R., & Saenger, W. (1988) *J. Biol. Chem. 263*, 15358–15368.

Crowther, R. A. (1972) in *The Molecular Replacement Method* (Rossmann, M. G., Ed.) pp 173–178, Gordon and Breach, Science Publishers, New York.

Evans, H. T., Jr. (1960) *Z. Kristallogr. 114*, 257–277.

Finzel, B. C. (1987) *J. Appl. Crystallogr. 20*, 53–55.

Fülling, R., & Rüterjans, H. (1978) *FEBS Lett. 88*, 279–282.

Hendrickson, W. A. (1985) in *Methods Enzymol. 115*, 252–270.

Hendrickson, W. A., & Konnert, J. H. (1980) in *Computing in Crystallography* (Diamond, R., Ramaseshan, S., & Venkatesan, K., Eds.) pp 13.01–13.23, Indian Academy of Sciences, Bangalore.

Jones, T. A. (1978) *J. Appl. Crystallogr. 11*, 268–272.

Jones, T. A. (1985) *Methods Enzymol. 115*, 157–171.

Kabsch, W., & Sander, C. (1983) *Biopolymers 22*, 2577–2637.

Keller, E. (1988) SCHAKAL 88, Kristallographisches Institut der Albert-Ludwigs-Universität, Freiburg, FRG.

Koepke, J., Maslowska, M., Heinemann, U., & Saenger, W. (1989) *J. Mol. Biol. 206*, 475–488.

Luzzati, V. (1952) *Acta Crystallogr. 5*, 802–810.

Machin, P. A., Wonacott, A. J., & Moss, D. (1983) *Daresbury News 10*, 3–9.

MacKerell, A. D., Jr., Nilsson, L., Rigler, R., & Saenger, W. (1988) *Biochemistry 27*, 4547–4556.

Martin, P. D., Tulinsky, A., & Walz, F. G., Jr. (1980) *J. Mol. Biol. 136*, 95–97.

Molecular Modelling System (1987) BIOSYM Technologies Inc., San Diego.

Pace, C. N., & Grimsley, G. R. (1988) *Biochemistry 27*, 3242–3246.

Pope, M. T., & Dale, B. W. (1968) *Q. Rev. Chem. Soc. 22*, 527–548.

Sheriff, S. (1987) *J. Appl. Crystallogr. 20*, 55–57.

Sugio, S., Amisaki, T., Ohishi, H., Tomita, K., Heinemann, U., & Saenger, W. (1985a) *FEBS Lett. 181*, 129–132.

Sugio, S., Oka, K., Ohishi, H., Tomita, K., & Saenger, W. (1985b) *FEBS Lett. 183*, 115-118.
Sugio, S., Amisaki, T., Ohishi, H., & Tomita, K. (1988) *J. Biochem. 103*, 354-366.
Wlodawer, A., Miller, M., & Sjölin, L. (1983) *Proc. Natl. Acad. Sci. U.S.A. 80*, 3628-3631.
Yu, H.-A., Karplus, M., & Hendrickson, W. A. (1985) *Acta Crystallogr. B41*, 191-201.

Structural Analysis of Specificity: α-Lytic Protease Complexes with Analogues of Reaction Intermediates†,‡

Roger Bone,§ Dan Frank,§ Charles A. Kettner,∥ and David A. Agard*,§

Department of Biochemistry and Biophysics and The Howard Hughes Medical Institute, University of California at San Francisco, San Francisco, California 94143-0448, and Central Research and Development Department, Experimental Station, E. I. du Pont de Nemours and Company, Inc., Wilmington, Delaware 19898

Received December 27, 1988; Revised Manuscript Received May 10, 1989

ABSTRACT: To better understand the structural basis of enzyme specificity, the structures of complexes formed between α-lytic protease, an extracellular serine protease of *Lysobacter enzymogenes*, and five inhibitory peptide boronic acids (R_2-boroX, where R_2 is methoxysuccinyl-Ala-Ala-Pro- and boroX is the α-aminoboronic acid analogue of Ala, Val, Ile, Norleu, or Phe) have been studied at high resolution by X-ray crystallography. The enzyme has primary specificity for Ala in the P_1 position of peptide substrates with catalytic efficiency decreasing with increasing side-chain volume. Enzyme affinity for inhibitors with boroVal, boroIle, and boroPhe residues is much higher than expected on the basis of the catalytic efficiencies of homologous substrates. Covalent tetrahedral adducts are formed between the active-site serine and the boronic acid moieties of R_2-boroAla, R_2-boroVal R_2-boroIle, and R_2-boroNorleu. Though R_2-boroVal is a slowly bound inhibitor and R_2-boroAla is rapidly bound [Kettner, C. A., Bone, R., Agard, D. A., & Bachovchin, W. W. (1988) *Biochemistry 27*, 7682-7688], there appear to be no structural differences that could account for slow binding. The removal from solution of 20% more hydrophobic surface on binding accounts for the improved affinity of α-lytic protease for R_2-boroVal relative to R_2-boroAla. The high affinity of the enzyme for R_2-boroIle derives from the selective binding of the L-allo stereoisomer of the boroIle residue, which can avoid bad steric interactions in the binding pocket. While R_2-boroNorleu buries as much hydrophobic surface as R_2-boroVal, its larger side chain causes alterations in enzyme conformation and inhibitor position, leading to a distortion of hydrogen bonds between the enzyme and inhibitor. A trigonal adduct is formed between the active-site serine and the boronic acid moiety of R_2-boroPhe in which the catalytic histidine occupies a position axial to the plane of the trigonal adduct. The histidine $N_{\epsilon 2}$ is 2.2 Å from the boron, suggesting that a coordinate covalent bond has formed.

One of the fundamental functions of an enzyme is to provide specificity by limiting the range of substrates that are catalytically productive. Since catalysis is a result of an enzyme's ability to bind the transition state for a reaction (Wolfenden, 1972), specificity must derive in large part from the selective binding of transition states for the reactions of favored substrates (Fersht, 1977). Studies relating catalytic efficiency to substrate structure serve to identify the important determinants of specificity residing on the substrate (Fersht, 1977). Similarly, site-directed mutagenesis can be used to determine which residues on the enzyme contribute to specificity (Estell et al., 1986). However, a thorough understanding of the interaction of these important structural elements, contributed by both the enzyme and substrate, can only be achieved through direct structural analysis. Of greatest interest are the structures of enzyme–substrate complexes during the transition state, since determinations of k_{cat}/K_M relate most closely to these structures (Fersht, 1977). While the structure of the transition state itself is inaccessible, the structures of enzyme complexes with analogues of the transition state can be determined. Crystallographic analysis of a series of complexes with systematically varying analogues should provide detailed structural information concerning which interactions are utilized in stabilizing good substrates and which interactions are disrupted with poor substrates. In addition, these structures could be useful as models for other types of molecular recognition such as the binding of ligands by receptors. In this work we report the determination by high-resolution X-ray crystallography of the structures of five enzyme–inhibitor complexes between α-lytic protease and a series of peptide boronic acids varying in the side chain of the boronic acid.

α-Lytic protease is an extracellular serine protease produced by the soil microorganism *Lysobacter enzymogenes*, apparently to bring about the lysis of microbes and small organisms also found in soil (Whitaker, 1970). The enzyme has been extensively studied as a model serine protease largely because it contains a single histidine residue located at the active site, which has facilitated magnetic resonance investigations of the pK_a values of the catalytic residues (Robillard & Schulman,

†This work was supported by funds from the Howard Hughes Medical Institute and from an NSF Presidential Young Investigator grant (D.A.A.). R.B. was supported by NIH National Research Service Award GM11174-02.

‡The atomic coordinates in this paper have been submitted to the Brookhaven Data Bank.

*Author to whom correspondence should be addressed.
§University of California at San Francisco.
∥E. I. du Pont de Nemours and Co., Inc.

0006-2960/89/0428-7600$01.50/0